Society of Exploration Geophysicists

June 7, 2004

Andries Wever
c/o Jura 22
NL-7607 RG Almelo
The Netherlands

Dear Mr. Andries Wever:

On behalf of the SEG/Denver 2004 Technical Program Committee, we would like to invite you to present your paper, *Criteria for source and receiver positioning in time-lapse seismic acquisition* at the SEG International Exposition and Seventy-Fourth Annual Meeting in Denver, CO. Your paper is scheduled for PC-Based presentation on Thursday, October 14, 2004.

All submitted papers were carefully reviewed by people with expertise in the appropriate area of geophysics and were rated on the basis of the submitted abstract and accompanying figures. The reviewers felt that your abstract represents a significant technical contribution that will be of interest to many Society members.

The full Committee met in May to arrange the presentations into sessions with a clear theme and focus. Your paper has been included in the 'TL 4: Novel Methodologies' session, which begins at 8:30 AM. Your 20-minute presentation will begin at 10:10 AM. The entire SEG/Denver 2004 Technical Program will be posted online at http://meeting.seg.org/techprog beginning August 1, 2004. I encourage you to take a look at the other papers in your session.

Please review the enclosed Speaker Kit. It contains: guidelines for preparing your presentation, information regarding the Speaker Breakfast and Student Paper competition, sample judging forms, tips for presenting your paper, and other pertinent information.

Now that your paper has been accepted, you are obligated to show up at the assigned time to give your presentation. People who do not show up to give their talk significantly disrupt the flow of the session, and are performing a great disservice to the other speakers in the session and the audience. SEG may impose a penalty on speakers who do not show up for their scheduled presentation. If you are unable to show up for your designated time, you must inform the SEG Technical Program Coordinator at ease@seg.org at least six weeks in advance of the meeting. Please don't be a "no-show!"

Again, thank you for your interest in presenting your work at the SEG Annual Meeting. You will help to make the Annual Meeting a significant learning experience for everyone. See you at the Speaker Breakfast!

Sincerely,

Scott MacKay

Dr. Scott MacKay
Technical Program Chairman

Enclosures
Reference No. 201

Criteria for source and receiver positioning in time-lapse seismic acquisition

Andries Wever and Jesper Spetzler, Dept. of Geotechnology, TU-Delft, The Netherlands*

Summary

The effects of mis-positioning in time-lapse seismics are studied, focusing on irregular sampling due to receiver mis-positioning and absence of data due to surface obstacles. Wavefield reconstruction is used to regularize data and to reconstruct data where data-gaps are present. The method is tested on time-lapse 2D synthetic and Troll streamer data. Quality control is performed using conventional difference plots, NRMS percentage and the 4D attributes reflection coefficient ratio and two-way travel-time shift.

Introduction

In time-lapse (4D) seismic acquisition, a monitor trace should ideally be recorded at exactly the same geographical position as the corresponding reference trace. However, in practice this is rarely the case, since in marine seismics 4D positioning errors are introduced in the data. These errors contain a known and an unknown component: the differential GPS system can give a monitor location that deviates significantly from the reference one. In addition, navigational uncertainties and positioning uncertainties along the streamers (due to cable feathering) are present in the data. Although stacking and binning might eliminate parts of this problem, the errors will still affect pre-stack processing such as NMO, DMO and pre-stack depth migration.

Methodology

The 4D positioning problem can be expressed as $x_B = x_A + x_{B-A} + \Delta x_r$, where x_A and x_B denote the reference and monitor trace position, x_{B-A} is the known deviation between the reference and monitor trace and Δx_r is the unknown error caused by the positioning uncertainty. After wavefield reconstruction using Fourier reconstruction with sparse inversion (FRSI) (Zwartjes and Duijndam, 2000) to correct for the known errors, the problem simplifies to $x_B = x_A + \Delta x_r$. These data (after FRSI) can be pre-stack processed and 4D evaluated.

To quantify the trade-off between production and acquisition, the propagation of the signal is analyzed through a homogeneous overburden and a reservoir layer (see Fig. 1). The reference two-way travel-time (*twt*) and acquisition effects in terms of *twt* are analyzed for receiver positioning errors Δx_r using simple ray-tracing and first-order perturbation theory. The production is modeled with the P-wave velocity change instead of a saturation change, as the Gassmann-equation shows nonlinear behavior. Then, to obtain expressions of the form $|\Delta\ twt_{prod}(x_r, \Delta S_{oil})| > |\Delta\ twt_{acq}(x_r, \Delta x_r)|$, one can derive for the *twt* difference due to either acquisition or production (with $\Delta v_2 = v_{mon,2} - v_{ref,2}$, subscript 1 for cap rock, 2 for reservoir) :

$$|\Delta twt_{acq}(x_r, \Delta x_r)| = \frac{1}{2v_{ref,1}\sqrt{\frac{1}{4}x_r^2 + D^2}}|x_r \Delta x_r| \quad (1)$$

and

$$|\Delta twt_{prod}(x_r, \Delta S_{oil})| = \frac{\sqrt{\frac{1}{4}x_{res}^2 + D_{res}^2}}{v_{ref,2}^2}|\Delta v_2|, \quad (2)$$

and using $D_{res}/D = \sqrt{\frac{1}{4}x_{res}^2 + D_{res}^2}/\sqrt{\frac{1}{4}x^2 + D^2}$ this can be simplified to:

$$|\Delta v_2| > \frac{v_{ref,2}^2}{2v_{ref,1}\left(\frac{1}{4}x_r^2 + D^2\right)\frac{D_{res}}{D}}|x_r \Delta x_r|. \quad (3)$$

In a similar vein, a detectability criteria based on the angle-dependent reflection change has been derived. To detect a production-induced P-wave velocity change $\Delta v_{P,2}$ under the top reservoir, it is found that

$$|\Delta v_{P,2}| > \frac{G}{2aD_{ob}^2}|x_r \Delta x_r|, \quad (4)$$

where G is the AVO-gradient (Mavko et al., 1998), D_{ob} is indicated in Fig. 1 and a is given by

$$a = \frac{5}{2}\frac{v_{P,1}}{(v_{P,2}+v_{P,1})^2} - \sin^2\left[4\langle v_S\rangle^2\frac{4v_{P,1}-2v_{P,2}}{(v_{P,1}+v_{P,2})^4} - 32\frac{\langle v_S\rangle\delta v_S}{(v_{P,1}+v_{P,2})^3} - 2\frac{v_{P,1}}{(v_{P,1}+v_{P,2})^2}\right]. \quad (5)$$

If the inequality represented by Eqs. (3) and (4) is fulfilled, the effect of production on traveltime or reflectivity is larger than the effect inherent to receiver mis-positioning. Both equations also show the offset and geology dependent impact of receiver mis-positioning. The offset-dependent behavior is important for AVO/AVA techniques as data from different offsets are compared although they are differently affected by the same positioning error.

To link production effects due to saturation change with acquisition effects inherent to receiver mis-positioning, normalized root-mean-square (NRMS) percentages are used. According to (Kragh and Christie, 2002), NRMS is defined as:

$$NRMS = \frac{RMS(a_t - b_t)}{RMS(a_t) + RMS(b_t)}\ 200(\%), \quad (6)$$

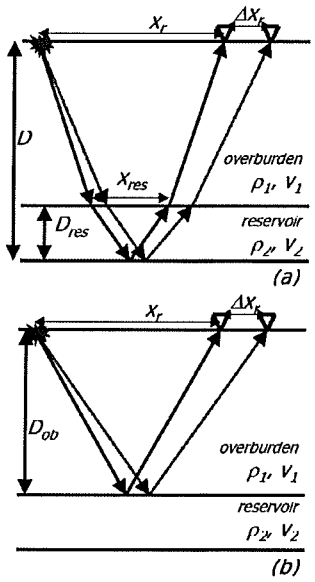

Fig. 1: Configuration and notation for detectability criteria derivations: (a) for $R(\theta)$and (b) for *twt*.

where the root-mean-squared function RMS of the time-series x_t is given by

$$RMS\,(x_i) = \sqrt{\frac{\sum_{t_1}^{t_2}(x_t)^2}{N}}, \qquad (7)$$

and is regularly applied on time-intervals $t_1 - t_2$ in the overburden, to quantify the difference of two data sets. However, NRMS can also be used to quantify the difference over small intervals (e.g. the reservoir). By doing so, the actual change in the reservoir, or even over a certain reflector of the reservoir, can be evaluated. If the production effects in terms of NRMS are then larger than the acquisition effects in terms of NRMS, the production should be detectable. This principle is used to merge the data from the acquisition and production analysis to obtain detectability criteria.

To model the *twt* difference due to production, the P-wave velocities are calculated by means of the Gassmann equation. Using the offset-dependent propagation length through the reservoir and the P-wave velocity difference, the production-induced *twt* difference $(\Delta twt_{prod}(x, \Delta S_{oil}))$ is calculated. The *twt* difference due to receiver mis-positioning is obtained by ray-tracing in the model for offsets x_r. Around x_r, receiver mis-positioning Δx_r is modeled by ray-tracing $(x_r + \Delta x_r)$. For the acquisition-induced time-lapse difference, it is then found that $\Delta twt_{acq}(x, \Delta x_r) = twt_{x_r+\Delta x_r} - twt_{x_r}$. For every point $(x_r, \Delta x_r)$ in the acquisition matrix, the saturation change $\Delta S_{oil}(x)$ causing an identical *twt* is calculated and stored in the production matrix. After convolution with a wavelet, the *twt* differences can be converted into NRMS values using a reflectivity panel. By plotting the acquisition matrix with colors and the production matrix as contours in the same plot, the trade-off between acquisition errors and expected production effects can be evaluated in terms of NRMS (see Fig. 2a). Fig. 2b is created following an analogue procedure, using the Zoeppritz equation to analyze the effect of receiver mis-positioning on the angle-dependent reflection strength.

Using a 2D geologic model representing a Viking-Trough setting, 120 shots are generated using fully-elastically 4^{th} order finite-difference modeling. This yields simulated pre-stack seismic data with shot and receiver (bin) spacing of 25 meter. In the final data, both known and unknown positioning errors are introduced (i.e. all traces have erroneous header values) resulting in a Gaussian distributed mis-positioning (Δx_r^{max} = 6m). After FRSI to correct for x_{B-A}, common-offset sections are extracted. In these common-offset sections, data gaps are introduced to simulate the absence of data due to surface obstacles (such as platforms). FRSI is again applied to fill the data gaps and the 4D attributes *reflection coefficient ratio* RCR and *twt* are separately extracted from the data using the convolution/deconvolution method, see (Spetzler and Kvam, 2003). The sections are then analyzed in terms of conventional seismic difference, NRMS, RCR and *twt* difference.

Numerical Modeling Results

Fig. 2 presents the results of the numerical modeling for two separate time-lapse attributes, left for *twt* and right for reflection. Note the strong difference in NRMS scale: whereas receiver mis-positioning up to 25 meter (at 3500m offset) causes NRMS differences up to 11% for the reflection, this causes up to 130% for *twt*. The saturation decrease that causes the same change in terms of NRMS shows the same trend, as becomes clear from the contours. If $\Delta x_r = 25m$, this corresponds for *twt* with a ΔS_{oil} of 80% and for reflection with only 4%.

Interpretation of the plot is straightforward: if an average receiver mis-positioning of 10 meter is considered for the *twt* case, one should evaluate a vertical line through $\Delta x_r = 10$. On the right side of this line, NRMS values of the acquisition (the color scale) and production (contours) continue to increase, on the left side they both decrease. This means that production features on the right side of this line will be detectable as their effect in terms of NRMS, will prevail over the acquisition NRMS given by the vertical line. For example, this line intersects the 0.8 curve at 500 meter and the 0.6 curve at 3500 and 1375 meter. Hence, given a mis-positioning of 10 meter at 500 meter offset, only saturation changes bigger than 20% (100 to 80%) would be detectable. The fact that a Δx_r line can intersect a saturation contour twice can be explained with the different offset-dependent effect on *twt* of saturation and mis-positioning. The saturation change shows an exponential behavior whereas the acquisition shows an asymptotic behavior in terms of NRMS.

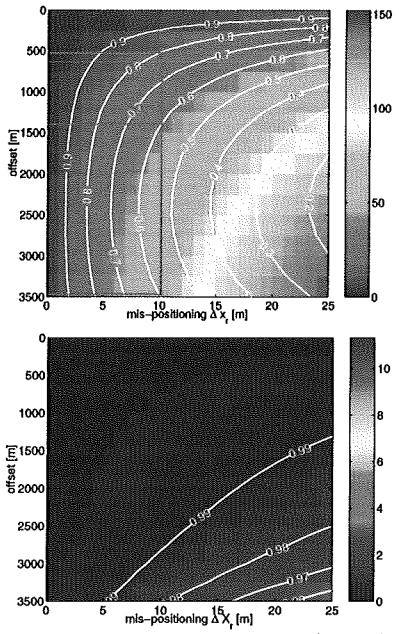

Fig. 2: Numerical modeling results for (a, left) *twt* and (b, right) $R(\theta)$ as a function of offset x_r and receiver mispositioning Δx_r for the base reservoir reflector. Colors indicate acquisition effects, contours represent production effects. Both are expressed in NRMS. Values at contours represent oil-saturations.

2D Synthetic and Real Data Results

As the 2D synthetic time-lapse data not only contained production-induced changes but also source-wavelet differences, overburden velocity differences and non-repeatable acquisition, the raw seismic difference is extremely strong, almost a shot record on its own, see Fig. 3a. This strong raw seismic difference also explains the high NRMS values of Fig. 3b. Although the raw seismic difference or NRMS graph do not enable the identification of production zones, both the reflection ratio and *twt* do, as shown in Fig. 4a and 4b. Especially in the semi-1D area, from 3300 to 3900 meter, the results are very good, although a reconstructed data gap is present here. A stable and reliable RCR is found that is validated with theoretically expected values. Also the structurally more complex part from 3000 to 3300 meter yields good results, both for the top and base reservoir reflector. The data reconstruction in the gap in the dipping part of the reservoir yields poor results. This could be due to limited dipping energy in the panel that is used in the wavefield reconstruction. The area 2500 to 3000 meter proves difficult, both due to the reconstructed dipping reflectors and wavelet tuning effects in the stratigraphic trap. Lastly, note that the offset dependent behavior has improved considerably for the reflection ratio and the traveltime compared with the NRMS values.

A real-data verification on single-fold time-lapse Troll streamer data yields comparable results. Although very high NRMS values are found, RCR and Δtwt identify some coherent trends on (semi-)horizontal reflectors.

Conclusions

It is demonstrated that the effect of receiver mispositioning in 4D seismics can be evaluated analytically and numerically. Plots can be composed representing acceptable receiver mis-positioning with respect to anticipated time-lapse saturation change. Such maps can help the survey designer to make relevant acquisition requirements for repeated surveys based on anticipated saturation changes at target depth. The plots provide the interpreter with a tool to estimate the reliability of an observed time-lapse change, given the accuracy of the survey. Using this knowledge, it is shown that it is possible to extract the time-lapse differences from a 2D synthetic pre-stack dataset without much pre-processing. Although the dataset contains severely non-repeatable features (such as source wavelet differences, overburden velocity changes and receiver positioning errors), it proved possible to exploit the different sensitivities of time-lapse attributes. By separate extraction of 4D attributes using the convolution/deconvolution method, it proved possible to estimate time-lapse changes more reliable. At the same time, Fourier reconstruction and sparse inversion proved valuable tools to improve data that contain considerable known and unknown positioning errors as well as to enhance data coverage. Verification on a real data set shows that the 4D attributes RCR and Δtwt indeed enable more reliable estimation of change.

Acknowledgments

This work is sponsored by the European Community through the Atlass project, no. NNE5-1999-20211. Norsk Hydro is acknowledged for the Troll data.

References

Kragh, E., and Christie, P., 2002, Seismic repeatability, normalised rms and predictability: The Leading Edge, **21**, 640–647.

Mavko, G., Mukerij, T., and Dvorkin, J., 1998, Teh rock physics handbook: Cambridge University Press.

Spetzler, J., and Kvam, O., 2003, Time-lapse monitoring in the prestack domain: 73rd, Soc. of Expl. Geophys. 1414–1417.

Zwartjes, P., and Duijndam, A., 2000, Optimizing reconstruction for sparse spatial sampling: 70, Soc. of Expl. Geophys. 2162–2165.

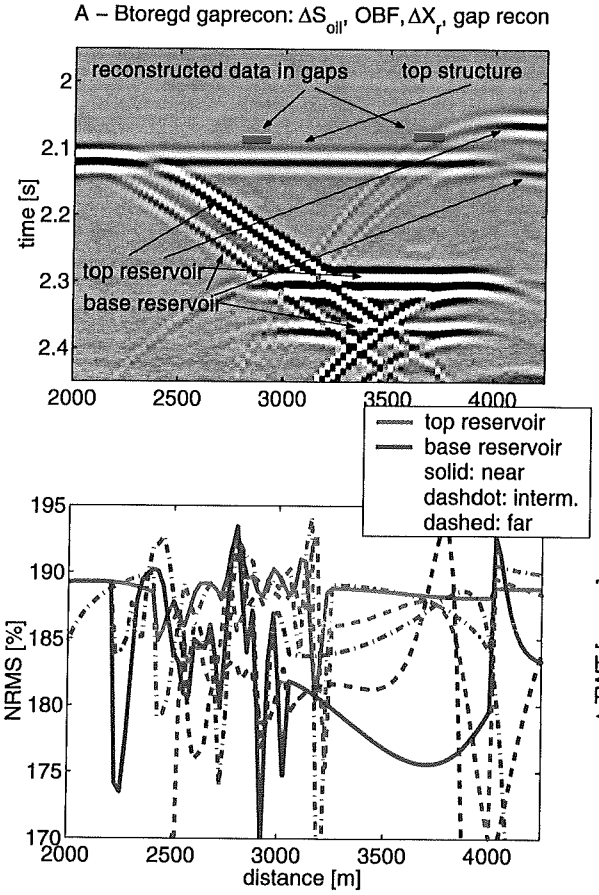

Fig. 3: Data after regularization and gap reconstruction (target oriented): (a, top) seismic difference display (near offset, 150 meter), (b, bottom) in terms of NRMS.

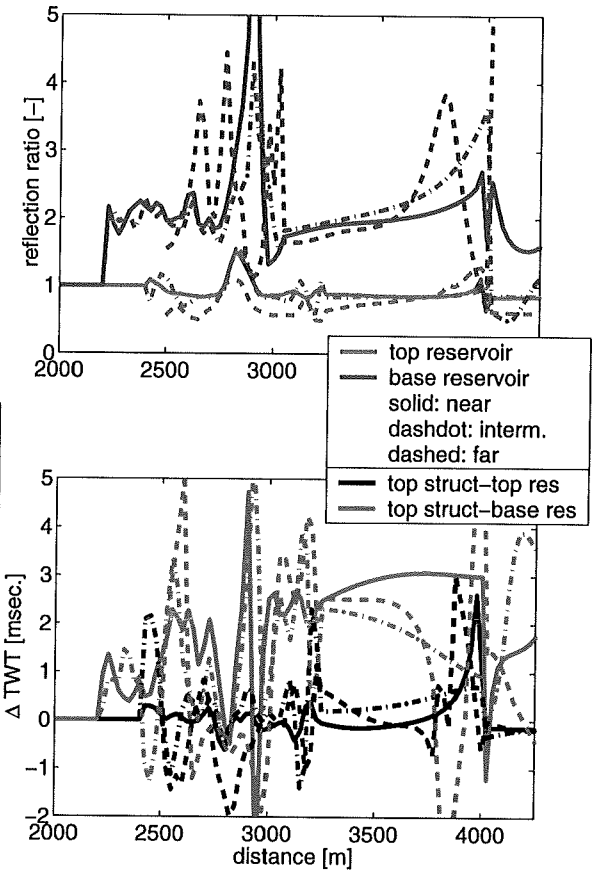

Fig. 4: Data after regularization and gap reconstruction (target oriented): (a, top) in terms of reflection ratio and (b, bottom) in terms of Δtwt. Near offset is 150 meter, intermediate 1000 and far 2000.